Research Article

ADVANCED PHOTONICS NEXUS

Generation of high-efficiency, high-purity, and broadband Laguerre-Gaussian modes from a Janus optical parametric oscillator

Dunzhao Wei,[a,b,†] Pengcheng Chen,[a,†] Yipeng Zhang,[a,†] Wenzhe Yao,[a] Rui Ni,[a] Xiaopeng Hu,[a,c] Xinjie Lv,[a,c] Shining Zhu,[a,c] Min Xiao,[a,c,d] and Yong Zhang[a,c,*]

[a]Nanjing University, College of Engineering and Applied Sciences, School of Physics, National Laboratory of Solid State Microstructures, Nanjing, China
[b]Sun Yat-Sen University, School of Physics, State Key Laboratory of Optoelectronic Materials and Technologies, Guangzhou, China
[c]Nanjing University, Collaborative Innovation Center of Advanced Microstructures, Nanjing, China
[d]University of Arkansas, Department of Physics, Fayetteville, Arkansas, United States

Abstract. Laguerre-Gaussian (LG) modes, carrying the orbital angular momentum of light, are critical for important applications, such as high-capacity optical communications, superresolution imaging, and multidimensional quantum entanglement. Advanced developments in these applications demand reliable and tunable LG mode laser sources, which, however, do not yet exist. Here, we experimentally demonstrate highly efficient, highly pure, broadly tunable, and topological-charge-controllable LG modes from a Janus optical parametric oscillator (OPO). The Janus OPO featuring a two-faced cavity mode is designed to guarantee an efficient evolution from a Gaussian-shaped fundamental pump mode to a desired LG parametric mode. The output LG mode has a tunable wavelength between 1.5 and 1.6 μm with a conversion efficiency >15%, a controllable topological charge up to 4, and a mode purity as high as 97%, which provides a high-performance solid-state light source for high-end demands in multidimensional multiplexing/demultiplexing, control of spin-orbital coupling between light and atoms, and so on.

Keywords: orbital angular momentum; Laguerre-Gaussian mode; optical parametric oscillator.

Received Dec. 28, 2022; revised manuscript received Mar. 7, 2023; accepted for publication Apr. 3, 2023; published online Apr. 21, 2023.

[DOI: 10.1117/1.APN.2.3.036007]

1 Introduction

Laguerre-Gaussian (LG) modes with unique spiral wavefronts are the paraxial solutions of the scalar Helmholtz equation in cylindrical coordinates, which can be distinguished by an azimuthal index l and a radial index p, i.e., $\mathrm{LG}(l, p)$. In 1992, Allen et al. demonstrated that an LG mode carries an orbital angular momentum (OAM) of $l\hbar$ per photon,[1] where l is called the topological charge (TC). Their pioneering work has significantly boosted the applications of LG modes from optical trapping and optical tweezer to optical communications, superresolution imaging, precision measurement, quantum information processing, and so on.[2–9] In turn, these high-end demands have triggered the developments of LG-mode laser sources in recent years.[10–17] Almost all the applications benefit from the high purity of an LG laser source, such as improved signal-to-noise ratio in rotation measurement, enhanced resolution in fluorescence imaging, and optimized coupling with an OAM photonic chip.[18–20] High-power laser output of LG mode could provide an effective way to decrease thermal noises in gravitational-wave detection.[21] In particular, LG laser sources are expected to be wavelength-tunable for wavelength division multiplexing in OAM-based high-capacity optical communication, investigation of spin-orbital coupling with various atoms in quantum storage and isolation, and excitations of versatile fluorescence in superresolution imaging.[19,22–25] However, these advanced applications are severely hampered by the limited wavelength bandwidth and mode purity in previous LG mode lasers. A reliable and broadband-tunable LG mode laser source does not yet exist.

*Address all correspondence to Yong Zhang, zhangyong@nju.edu.cn

†These authors contribute equally to this work.

The optical parametric oscillator (OPO) has been recognized as one of the most popular tunable sources.[26–29] A pump wave with frequency of ω_p generates two parametric waves,[30] i.e., signal and idler waves at the frequencies of ω_s and ω_i, respectively, through the second-order nonlinear downconversion process. It satisfies the energy conservation of $\omega_p = \omega_i + \omega_s$. By controlling the phase-matching condition for momentum conservation, one can obtain wavelength-tunable output of the generated parametric waves.[31] An OPO system is capable of outputting broad wavelengths covering ultraviolet (UV), visible, and infrared bands, which makes it an excellent candidate for broadband output of high-quality LG modes. There are two reported configurations. One is to build a traditional OPO outputting a Gaussian mode, and then convert it to an LG mode using a spiral phase plate, a fork grating, a Q-plate, a vector vortex waveplate (VVW), or a spatial light modulator [Fig. 1(a)].[6,32–35] Because these devices only introduce a spatial phase modulation, the generated beam is actually a superposition of various higher-order LG modes with the same azimuthal index l but a different radial index p, i.e., $\sum_p \mathrm{LG}(l, p)$. Although the conversion efficiency of a commercial device reaches 95%, it suffers from poor mode purity,[36,37] and generally, the higher the TC is, the lower mode purity becomes (typically 80% and 60% for LG(1, 0) and LG(2, 0) modes, respectively). See Note 1 in the Supplementary Material for details. The other approach is to oscillate an LG mode inside the OPO cavity [Fig. 1(b)] by utilizing the fact that

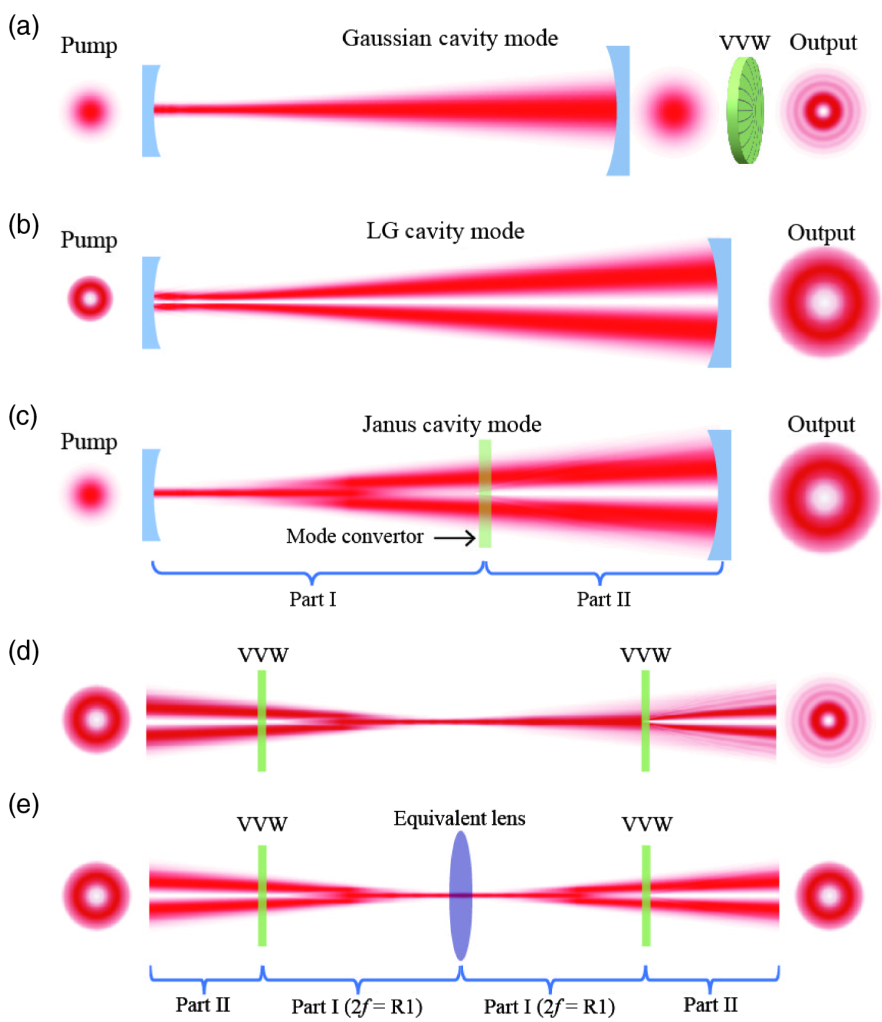

Fig. 1 Different cavity modes in OPO and Janus OPO designs. (a) A Gaussian-pumped OPO oscillating in a fundamental Gaussian mode. (b) An LG-pumped OPO with an LG cavity mode and an LG output mode. (c) A specially designed Janus OPO that is pumped by a Gaussian mode but outputs an LG mode. (d) A one-round-trip mode conversion without an imaging system. An LG mode passing through a VVW produces a hollow Gaussian beam, which evolves into a Gaussian-like mode after a certain propagation. However, the hollow Gaussian beam cannot recover itself without the equivalent lens as in panel (e) and neither can the LG mode. (e) A one-round-trip mode conversion inside a Janus OPO. The input coupler with a radius curvature of R1 can be seen as an equivalent lens with a focusing length of $2f = \mathrm{R1}$. Therefore, the light field after the VVW, which is set at the curvature center, will recover itself at the same position after being reflected by the input coupler.

LG modes are Eigen cavity modes,[38,39] which could also extend the output wavelength.[40] In comparison to a Gaussian-mode OPO system, the frequency conversion of an LG mode is less efficient because its donut-shaped profile has a much lower power density. In addition, the output mode quality is not as good as had been hoped. The fiber laser is another potential platform for broadband output of LG mode, but it suffers from low mode purity as well.[41,42]

Here, we propose and experimentally demonstrate a Janus OPO based on quasi-phase-matching (QPM) configuration[43–47] for highly efficient output of highly pure, broadly tunable, and TC-controllable LG modes [Fig. 1(c)]. The Janus cavity that we have previously studied features two-faced transverse-mode structures (like the god Janus in ancient Roman mythology), which combines the advantages of both Gaussian and LG cavity modes.[48] The nonlinear crystal, i.e., a periodically poled lithium niobate (PPLN) crystal, is set next to the front mirror to fully utilize the Gaussian-like front face of Janus cavity mode for high conversion efficiency. Most importantly, due to the introduction of an intracavity imaging system, the generated parametric light is naturally converted into a designed LG mode at the output port of the cavity. The cavity loss is significantly reduced because no additional spatial mode filter is used inside the cavity. The experimental results present a high-performance LG mode source beyond the existing methods. For the generated signal LG beam, the wavelength is tunable between 1.5 and 1.6 μm, the conversion efficiency is >15%, the TC is controllable up to 4, and most importantly, the mode purity can reach 97%.

2 Janus Cavity Theory

As shown in Fig. 1(c), the Janus cavity has a two-faced cavity mode, distinguishing itself from the traditional cavity mode configuration [Figs. 1(a) and 1(b)]. The front face at the input mirror has a Gaussian profile to achieve a better conversion efficiency because of its higher power density relative to the LG mode. The back face at the end mirror is a donut-shaped LG profile, which guarantees the direct output of a high-purity LG mode. The key question is how to smoothly evolve the cavity mode from a Gaussian profile to an LG profile, and vice versa, without breaking the cavity mode reversibility. The general idea is to directly put a spatial phase modulator, such as a VVW, into the cavity to complete the mode conversion.[14,49] However, phase modulation alone is not sufficient to perform a perfect spatial mode conversion due to lack of necessary amplitude modulation. Let us consider an ideal LG mode at the output mirror. As shown in Fig. 1(d), it propagates through the VVW, which produces a beam superimposed by multiple modes in Part I of the Janus OPO rather than a single mode, as in a traditional cavity.[50] This superimposed beam of multiple spatial modes hardly keeps its profile during free propagation. Therefore, the VVW alone cannot convert it back into the same LG mode as the initial one [Fig. 1(d)], which breaks the spatial mode reversibility inside the cavity. Under this situation, previous reports used an iris to filter out the unwanted high-order mode, which introduces a substantial cavity loss and severely limits laser performance.[14,49]

To realize an ideal Janus OPO [Fig. 1(c)], the mode reversibility has to be simultaneously satisfied for multiple modes in Part I of the cavity.[48] The key is to introduce an imaging system into the cavity. In our experiment, we use a concave front (input) mirror as an equivalent imaging lens for the compact Janus OPO design [Fig. 1(c)]. Figure 1(e) shows the transformation of Janus cavity mode in a round trip. When the imaging system works properly, the multiple spatial modes will repeat themselves after passing through the equivalent lens (i.e., being reflected back at the concave front mirror). Then, the VVW can convert them back into an ideal LG mode in Part II of the Janus OPO, and the reversibility condition inside the cavity can therefore be perfectly fulfilled in principle. In addition, the cavity mode profile near the front mirror is required to match the pump Gaussian mode. In our Janus cavity design, the multiple modes after an LG mode passing through the VVW compose a so-called hollow-Gaussian beam,[50] which naturally evolves into a spatial profile very close to a Gaussian mode after a certain propagation distance [Fig. 1(d)]. See Note 3 in the Supplementary Material for the detailed mathematics in designing a Janus cavity. In comparison to previous designs, all the spatial modes during mode conversion are fully utilized in such a Janus cavity. Therefore, the cavity loss greatly decreased and the output performance significantly improved.

3 Results

3.1 Experimental Setup of the Janus OPO

Figure 2(a) shows the experimental setup of a Janus OPO for generation of an LG-mode signal beam. Its output wavelength is designed to be tunable within the optical communication band. Two concave mirrors form the input and output couplers, which are coated for high reflectivity at the signal wavelength. A PPLN crystal serves as the nonlinear medium, which has multiple channels to extend the QPM bandwidth. The pump beam is generated by a 1064-nm pulsed nanosecond laser and focused into the crystal with a spot size of 200 μm in diameter, which matches the size of signal Gaussian-like face inside the crystal (see Note 4 in the Supplementary Material). Besides the Janus cavity mode as discussed above, the polarization of the field in the cavity is also precisely controlled to facilitate the parametric downconversion and mode conversion. In the PPLN crystal, both the pump and signal waves polarize vertically to utilize the biggest nonlinear coefficient d_{33} of the PPLN crystal for high conversion efficiency. By changing the temperature and selecting a channel of the PPLN crystal, the output wavelength of signal wave can range from 1480 to 1650 nm (see Note 2 in the Supplementary Material for the details). The next mode conversion subsystem includes a Faraday rotator (FR), a quarter-wave plate (QWP), and a VVW (the system has a work bandwidth of 1550 nm $\pm$ 50 nm). The VVW has a distinct q factor, with its value being a positive multiple of 1/2. In the forward propagation direction, a TC of $l = \pm 2q$ is loaded onto the signal wave, which will be canceled when it passes through the VVW again on its way back. To generate a high-purity LG mode at the output, the cavity mode in Part I should be reconfigured to form a superposition of multiple spatial modes, which is automatically achieved by the Janus cavity design. Here, we use a concave input coupler and set the VVW at its curvature center, which composes a symmetric imaging system to satisfy the condition of multimode reversibility in Part I of the Janus OPO [Fig. 1(e)]. In principle, an ideal LG mode propagates in Part II of the cavity. Such a stable Janus cavity mode is confirmed by numerical calculations based on the Fox–Li simulating process [Fig. 2(b)]. The cross sections of the Janus modes for different TCs show how a Gaussian-like mode is naturally transformed to a desired LG mode (See Appendix A and Note 4 in the Supplementary Material for the details). It should be noted that the mode

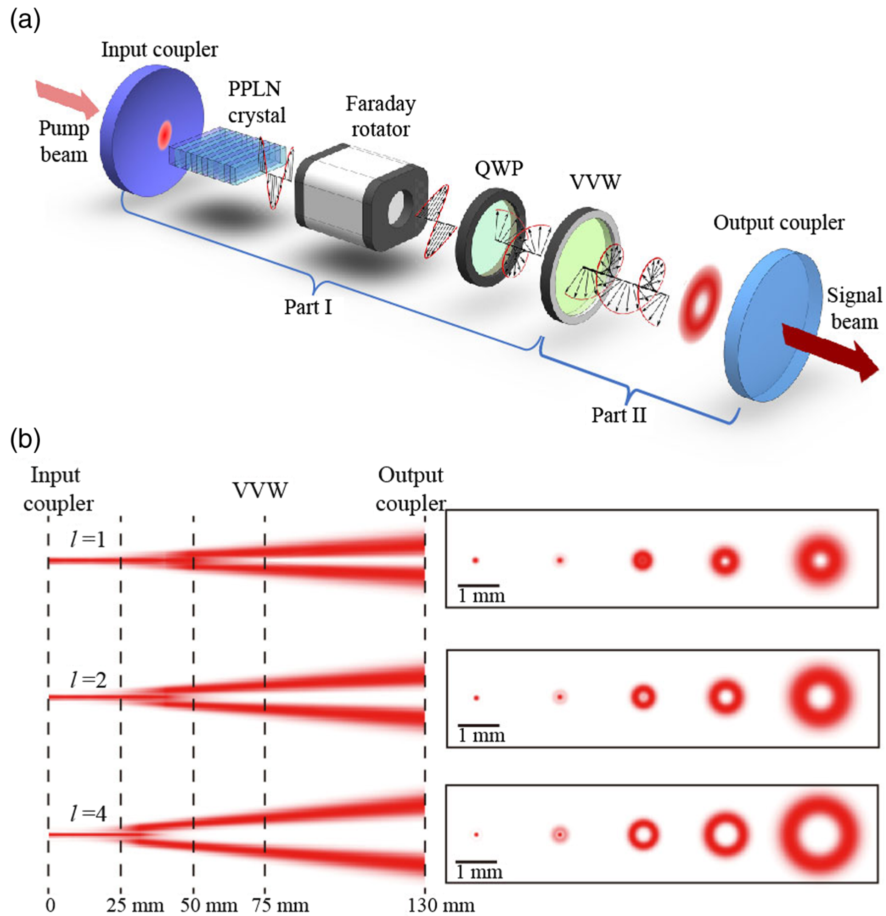

Fig. 2 Experimental setup and Janus mode simulation. (a) The PPLN crystal, as the nonlinear medium, transforms one pump photon into a signal photon and an idle photon through the QPM parametric downconversion process. The input/output couplers are coated for high reflectivity at the signal wavelength. The FR, QWP, and VVW form a mode conversion setup inside the cavity. The QWP alters the vertical polarization of the signal beam to circular polarization so that the spin-OAM conversion can happen on the VVW to achieve the desired Gaussian-to-LG mode conversion. The output LG mode can be changed by rotating the QWP or replacing the VVW. FR is used to keep the signal wave to be vertically polarized inside the PPLN crystal. (b) Janus cavity modes for $l = 1$, 2, and 4 and their cross sections at different distances of 0, 25, 50, 75, and 130 mm away from the input coupler.

conversion process requires a circularly polarized signal wave on the VVW. To fulfill the polarization reversibility in the cavity, we add an FR and a QWP to accomplish the polarization control (see Note 5 in the Supplementary Material for the details).

3.2 Performance of the Janus OPO

First, we demonstrate the generation of high-purity LG(1, 0) and LG(−1,0) modes. A VVW with $q = 1/2$ is used to introduce a TC of $l = \pm 1$. The sign is controlled by the orientation of the QWP. Under QPM configuration, the vertically polarized pump beam produces a vertically polarized signal beam in the PPLN crystal. After passing through the FR, the signal beam has a 45 deg linear polarization. When the fast axis of the QWP orients vertically (or horizontally), the signal polarization is further changed to a left- (or right-) circularly polarized one, resulting in $l = 1$ (or -1) after the VVW (Fig. 2) (see Note 5 in the Supplementary Material). The intensity patterns of the output LG(1, 0) and LG(−1,0) modes at 1550 nm showed in Figs. 3(a) and 3(b) exhibit high-quality donut intensity distribution without observable sidelobes. Clearly, the undesired higher-order LG modes ($p > 0$) are significantly suppressed by the Janus OPO cavity. Further modal analyses in Figs. 3(a) and 3(b) show that the generated LG(1, 0) and LG(−1,0) modes have mode purities of 96.6% and 97.0%, respectively (see Note 6 in the Supplementary Material for the modal analysis process). The mode purity is greatly enhanced in comparison to the typical value of ~80% using a VVW outside the cavity.[37] Our specially designed Janus OPO is also suitable for generating high-order, high-purity LG modes [Fig. 2(b)]. As a demonstration, VVWs of $q = 1$ and $q = 2$ are used to generate LG(±2,0) and LG(±4,0) modes. Since LG($\pm l$, 0) modes experience the similar transverse-mode evolution in the OPO, we only show the results of LG(2, 0) and LG(4, 0) modes [Figs. 3(c) and 3(d)]. The mode purities of 95.2% for the output LG(2, 0) mode and 93.7% for the LG(4, 0) mode are much superior to the 60% and 50% values

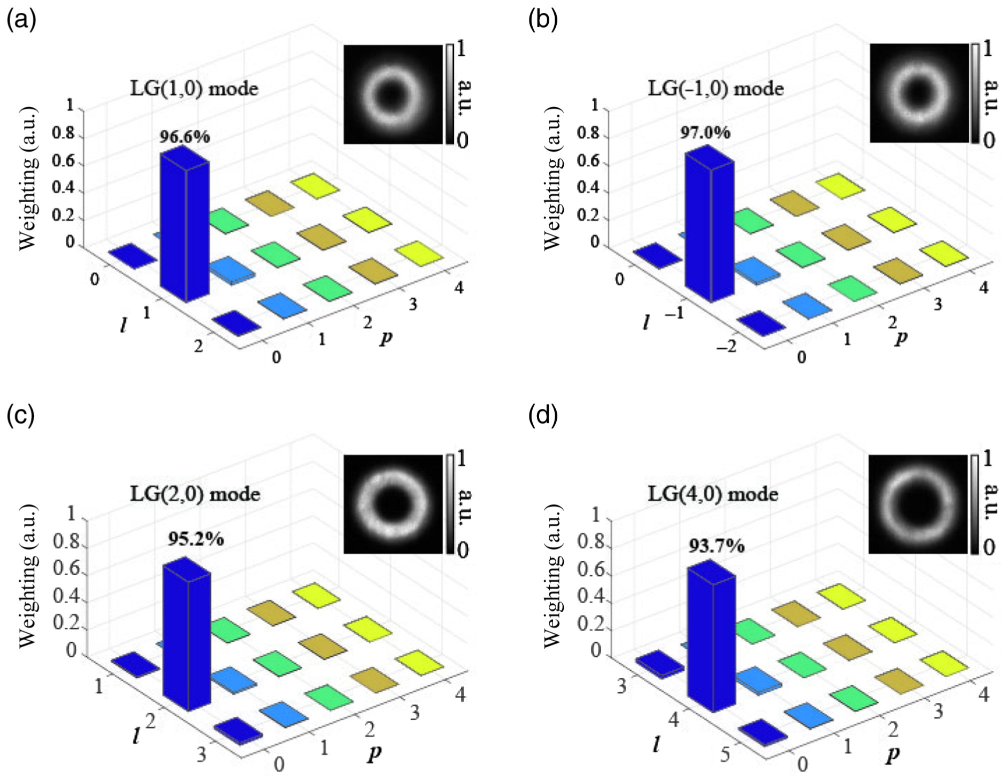

Fig. 3 TC-controllable generation of high-purity LG(l, 0) modes at the wavelength of 1550 nm. Modal analyses show high mode purities of 96.6%, 97.0%, 95.2%, and 93.7% for (a) LG(1, 0), (b) LG(−1, 0), (c) LG(2, 0), and (d) LG(4, 0) modes, respectively. The insets are the intensity patterns of the corresponding LG modes.

using VVWs outside the cavity.[37] It should be noted that the VVWs should be precisely collimated with the optical axis of the cavity to realize a high-purity output of LG modes. See Note 7 in the Supplementary Material for details.

In our experiment, the output wavelength of the Janus OPO can be tuned by changing the QPM channel and the temperature of the PPLN crystal. The Janus OPO shows excellent performance within the designed wavelengths ranging from 1500 to 1600 nm. As shown in Fig. 4(a), the conversion efficiency of the signal LG mode surpasses 10% in most of the working wavelengths. Under a pump power of 4.2 W, the conversion efficiencies for LG(1,0), LG(2, 0), and LG(4, 0) modes at 1550 nm reach 15.3%, 15.8%, and 15.6%, respectively. Notably, the Janus OPO maintains a high conversion efficiency for high-order LG modes. In comparison to the output performance of the signal Gaussian mode in a traditional OPO system [Fig. 4(a)], the slightly decreasing conversion efficiencies for the outputs of LG modes can be mainly attributed to the limited mode conversion efficiency of VVWs shown in Table S1 in the Supplementary Material and the reflection losses from the FR and QWP. Figure 4(b) compares the power dependence of the output LG(1,0) mode on the pump power at 1525, 1550, 1575, and 1600 nm, respectively, whose thresholds are 1.6, 1.1, 1.2, and 1.5 W, respectively. The differences in the threshold and conversion efficiency for different wavelengths can be attributed to the fact that the intracavity optical components are not uniformly optimized at all the wavelengths. Figure 4(c) depicts the modal analysis results of the output LG(1, 0) mode at the wavelengths of 1525 and 1575 nm, which show high mode purities of 97.1% and 95.9%, respectively. The bandwidth of this Janus OPO can be further extended using ultrawideband optical components as intracavity elements.

4 Discussion

We have proposed and experimentally demonstrated a Janus OPO system for generating highly efficient, highly pure, broadly tunable, and TC-controllable LG modes. Such a Janus OPO distinguishes itself by possessing a two-faced cavity mode, which makes use of the distinct advantages of both the Gaussian and LG cavity modes. The front (input) face has a Gaussian profile to achieve the high-efficiency nonlinear frequency conversion, while its back (output) face is a donut-shaped LG profile that guarantees the direct output of a desired high-purity LG mode from the cavity. The key to realizing such a Janus OPO is the introduction of an imaging system to facilitate the perfect intracavity mode conversion. In this work, the Janus OPO is designed for the Gaussian-to-LG mode conversion of the signal light, which can be easily adjusted to output an LG mode at the idler wavelength. The conversion efficiency of the Janus OPO could be further enhanced by use of a double-pass pump configuration.[47] In addition, by selecting proper optical components, our experimental configuration can be readily extended to visible and UV wavelength bands, as well as to generate tunable vector beams and multidimensional quantum entangled sources. The excellent features of the LG modes from our Janus OPO (e.g., wavelength tunable between

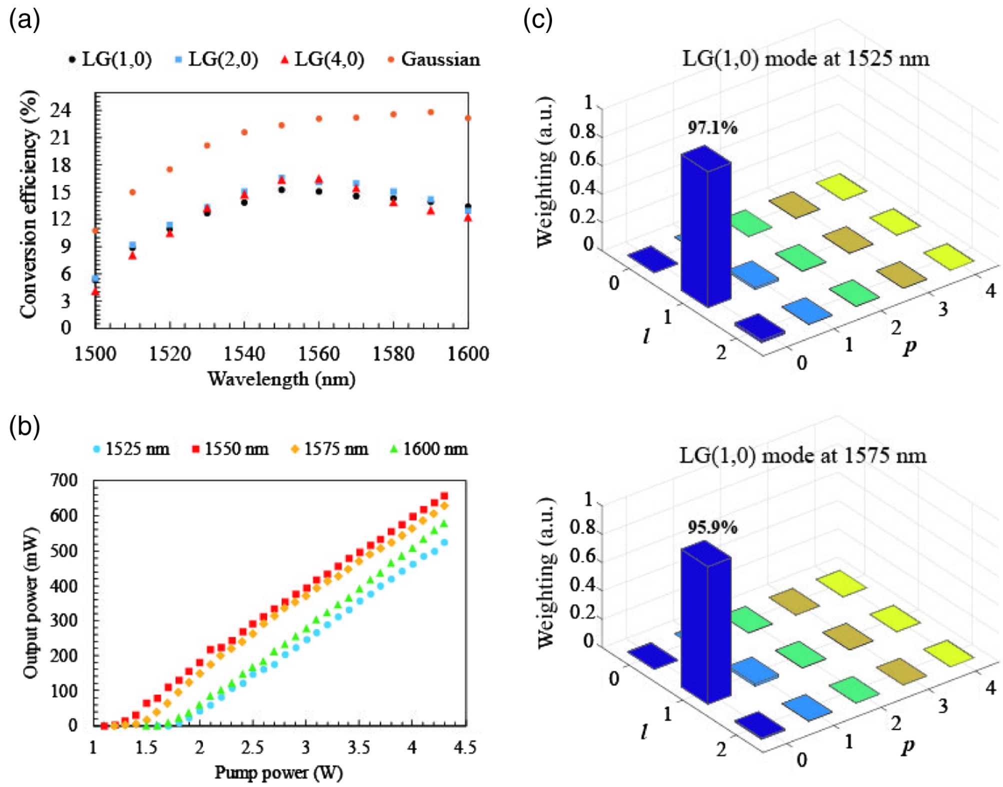

Fig. 4 Wavelength tunable high-purity LG modes. (a) Dependence of the conversion efficiencies of LG modes ($l = 1, 2, 4$) on the wavelength ranging from 1500 to 1600 nm at a pump power of 4.2 W, showing high conversion efficiencies at the designed bandwidth. (b) Dependences of output powers of LG(1, 0) mode on the pump power at 1525, 1550, 1575, and 1600 nm, respectively, showing high-quality OPO output performances. (c) Modal analysis for the output LG(1, 0) mode at the wavelengths of 1525 and 1575 nm, showing the mode purity up to 97.1%.

1.5 and 1.6 μm, conversion efficiency >15%, and mode purity >97%) can meet the critical requirements of high-level applications such as high-capacity optical communications, high-precision sensing and measurements, and superresolution imaging. In addition, the linewidth of LG modes could be narrowed using a continuous wave (CW) pump laser, enabling potential investigation of spin-orbital coupling with various atoms in quantum applications.

5 Appendix A: Experimental Setup

As shown in Fig. 2(a), a PPLN crystal with dimensions of $25(x) \times 12.3(y) \times 1(z)$ mm^3 serves as the nonlinear medium. Both of its end faces have a transmittance >99% in the 1380- to 1800-nm wavelength range. It is mounted inside an oven with the temperature tunability up to 150°C. The input coupler (with a radius of curvature of 75 mm) is coated with a high transmittance (>99%) at 1064 nm and a high reflectivity (>99%) at 1450 to 1650 nm, while the output coupler (with a radius of curvature of 125 mm) is coated with a transmittance of 30% at 1450 to 1650 nm. The cavity length is 140 mm, satisfying the stability condition of a resonator. A pump beam (wavelength of 1064 nm, repetition rate of 22 kHz, pulse width of 45 ns, linewidth of 5 nm) is generated by a nanosecond-pulsed fiber laser (YDFLP-M7-3-PM, JPT Co.). It is focused by a lens into a 200-μm-in-diameter spot inside the crystal. The PPLN crystal has 10 channels. In the experiment, we use four channels with periods of 31.02, 30.49, 29.98, and 29.52 μm, respectively. Under the pumping wavelength of 1064 nm, the output signal wave with a wavelength bandwidth of 1.4 nm (see Notes 2 and 8 in the Supplementary Material for details) can be tuned from 1480 to 1650 nm in the temperature range from 25°C to 138°C. An FR, a QWP, and a VVW are inserted into the cavity to achieve the reversible mode conversion inside the cavity. VVW is a spatially variant half-wave plate whose optical axis rotates continuously around a singularity point. All their working wavelength bandwidths are from 1500 to 1600 nm. The VVW is placed at a distance of 90 mm away from the input coupler, where the curvature center of the input coupler is, considering the effective length due to the high refractive index of the PPLN crystal. VVWs of $q = 0.5$, 1, 2 have been used to generate LG$(l, 0)$ modes with different TCs. The output intensity patterns are recorded by a laser beam profiler (LBP, Newport Corp.).

6 Appendix B: Cavity Mode Simulations

The numerical simulations have been carried out based on the Fox–Li method. A one-round-trip transition of the cavity mode can be described in what follows. A parametric wave starting from the input coupler travels a distance of L_A and passes through the VVW with a TC of l (or $-l$). After traveling a distance of L_B, the parametric wave is reflected by the output coupler and propagates backward. The TC is canceled when the parametric wave passes through the VVW along the opposite direction. Finally, the parametric wave reaches the input mirror to finish its one-round-trip transition. The parametric wave repeats the cycle until a stable cavity mode is formed. Base on angular spectrum theory, the iterative procedure described above is calculated step by step using MATLAB programming.

Acknowledgments

This work was supported by the National Key R&D Program of China (Grant No. 2021YFA1400803), the National Natural Science Foundation of China (Grant Nos. 91950206, 11874213, and 11674171), the Key Research Program of Jiangsu Province (Grant No. BE2015003-2), and the Guangdong Natural Science Funds for Distinguished Young Scholars (Grant No. 2022B1515020067).

Data Availability

The data that support the results within this paper and other findings of the study are available from the corresponding authors upon reasonable request.

Code Availability

The custom code and mathematical algorithm used to obtain the results within this paper are available from the corresponding authors upon reasonable request.

References

1. L. Allen et al., "Orbital angular momentum of light and the transformation of Laguerre-Gaussian laser modes," *Phys. Rev. A* **45**, 8185–8189 (1992).
2. Y. Shen et al., "Optical vortices 30 years on: OAM manipulation from topological charge to multiple singularities," *Light Sci. Appl.* **8**, 90 (2019).
3. Y. Yang et al., "Optical trapping with structured light: a review," *Adv. Photonics* **3**, 034001 (2021).
4. N. Bozinovic et al., "Terabit-scale orbital angular momentum mode division multiplexing in fibers," *Science* **340**, 1545–1548 (2013).
5. S. W. Hell, "Far-field optical nanoscopy," *Science* **316**, 1153–1158 (2007).
6. A. Mair et al., "Entanglement of the orbital angular momentum states of photons," *Nature* **412**, 313–316 (2001).
7. M. Erhard, M. Krenn, and A. Zeilinger, "Advances in high-dimensional quantum entanglement," *Nat. Rev. Phys.* **2**, 365–381 (2020).
8. Q. Jia et al., "Transferring linear motion of an optical wedge to rotational frequency shift in an orbital angular momentum interferometer," *Appl. Phys. Lett.* **111**, 091102 (2017).
9. V. D. Salakhutdinov, E. R. Eliel, and W. Loffler, "Full-field quantum correlations of spatially entangled photons," *Phys. Rev. Lett.* **108**, 173604 (2012).
10. M. Piccardo et al., "Vortex laser arrays with topological charge control and self-healing of defects," *Nat. Photonics* **16**, 359 (2022).
11. A. Forbes, "Structured light from lasers," *Laser Photonics Rev.* **13**, 1900140 (2019).
12. H. Sroor et al., "High-purity orbital angular momentum states from a visible metasurface laser," *Nat. Photonics* **14**, 498–503 (2020).
13. J. Fan et al., "Two-channel, dual-beam-mode, wavelength-tunable femtosecond optical parametric oscillator," *Adv. Photonics* **2**, 1 (2020).
14. D. Naidoo et al., "Controlled generation of higher-order Poincaré sphere beams from a laser," *Nat. Photonics* **10**, 327–332 (2016).
15. Z. Zhang et al., "Tunable topological charge vortex microlaser," *Science* **368**, 760–763 (2020).
16. X. Cai et al., "Integrated compact optical vortex beam emitters," *Science* **338**, 363–366 (2012).
17. P. Miao et al., "Orbital angular momentum microlaser," *Science* **353**, 464–467 (2016).
18. M. P. J. Lavery et al., "Detection of a spinning object using light's orbital angular momentum," *Science* **341**, 537–540 (2013).
19. B. Neupane, F. S. Ligler, and G. Wang, "Review of recent developments in stimulated emission depletion microscopy: applications on cell imaging," *J. Biomed. Opt.* **19**, 080901 (2014).
20. Y. Chen et al., "Mapping twisted light into and out of a photonic chip," *Phys. Rev. Lett.* **121**, 233602 (2018).
21. L. Carbone et al., "Generation of high-purity higher-order Laguerre-Gauss beams at high laser power," *Phys. Rev. Lett.* **110**, 251101 (2013).
22. A. Alexandrescu, D. Cojoc, and E. Di Fabrizio, "Mechanism of angular momentum exchange between molecules and Laguerre-Gaussian beams," *Phys. Rev. Lett.* **96**, 243001 (2006).
23. A. E. Willner et al., "Recent advances in high-capacity free-space optical and radio-frequency communications using orbital angular momentum multiplexing," *Phil. Trans. R. Soc. A* **375**, 20150439 (2017).
24. M. S. Kwon et al., "Direct transfer of light's orbital angular momentum onto a nonresonantly excited polariton superfluid," *Phys. Rev. Lett.* **122**, 045302 (2019).
25. N. Carlon Zambon et al., "Optically controlling the emission chirality of microlasers," *Nat. Photonics* **13**, 283–288 (2019).
26. N. E. Yu et al., "Efficient optical parametric oscillation based on periodically poled 1.0 mol% MgO-doped stoichiometric $LiTaO_3$," *Appl. Phys. Lett.* **85**, 5134–5136 (2004).
27. C. Canalias and V. Pasiskevicius, "Mirrorless optical parametric oscillator," *Nat. Photonics* **1**, 459–462 (2007).
28. F. Kienle et al., "High-power, high repetition-rate, green-pumped, picosecond LBO optical parametric oscillator," *Opt. Express* **20**, 7008–7014 (2012).
29. A. Marandi et al., "Network of time-multiplexed optical parametric oscillators as a coherent Ising machine," *Nat. Photonics* **8**, 937–942 (2014).
30. R. W. Boyd, *Nonlinear Optics*, 3rd ed., Academic Press (2008).
31. O. Gayer et al., "Temperature and wavelength dependent refractive index equations for MgO-doped congruent and stoichiometric $LiNbO_3$," *Appl. Phys. B* **91**, 343–348 (2008).
32. S. S. Oemrawsingh et al., "Production and characterization of spiral phase plates for optical wavelengths," *Appl. Opt.* **43**, 688–694 (2004).
33. M. Rafayelyan and E. Brasselet, "Spin-to-orbital angular momentum mapping of polychromatic light," *Phys. Rev. Lett.* **120**, 213903 (2018).
34. B. Y. Wei et al., "Generating switchable and reconfigurable optical vortices via photopatterning of liquid crystals," *Adv. Mater.* **26**, 1590–1595 (2014).
35. X. W. Wang et al., "Recent advances on optical vortex generation," *Nanophotonics* **7**, 1533–1556 (2018).
36. E. Karimi et al., "Hypergeometric-Gaussian modes," *Opt. Lett.* **32**, 3053–3055 (2007).
37. B. Sephton, A. Dudley, and A. Forbes, "Revealing the radial modes in vortex beams," *Appl. Opt.* **55**, 7830–7835 (2016).
38. K. Miyamoto et al., "Optical vortex pumped mid-infrared optical parametric oscillator," *Opt. Express* **19**, 12220–12226 (2011).
39. A. Aadhi et al., "Controlled switching of orbital angular momentum in an optical parametric oscillator," *Optica* **4**, 349 (2017).
40. T. Omatsu, K. Miyamoto, and A. J. Lee, "Wavelength-versatile optical vortex lasers," *J. Opt.* **19**, 123002 (2017).
41. N. Zhou, J. Liu, and J. Wang, "Reconfigurable and tunable twisted light laser," *Sci. Rep.* **8**, 11394 (2018).
42. J. Zou et al., "Green/red pulsed vortex-beam oscillations in all-fiber lasers with visible-resonance gold nanorods," *Nanoscale* **11**, 15991–16000 (2019).

43. C.-S. Yu and A. H. Kung, "Grazing-incidence periodically poled $LiNbO_3$ optical parametric oscillator," *J. Opt. Soc. Am. B* **16**, 2233–2238 (1999).
44. M. Lazoul et al., "Multi-resonant optical parametric oscillator based on 2D-PPLT nonlinear photonic crystal," *Opt. Lett.* **40**, 1861–1864 (2015).
45. U. Bäder et al., "Nanosecond periodically poled lithium niobate optical parametric generator pumped at 532 nm by a single-frequency passively Q-switched Nd:YAG laser," *Opt. Lett.* **24**, 1608–1610 (1999).
46. H. C. Guo et al., "Multiple-channel mid-infrared optical parametric oscillator in periodically poled MgO: $LiNbO_3$," *J. Appl. Phys.* **101**, 113112 (2007).
47. S. T. Yang, R. C. Eckardt, and R. L. Byer, "Continuous-wave singly resonant optical parametric oscillator pumped by a single-frequency resonantly doubled Nd:YAG laser," *Opt. Lett.* **18**, 971–973 (1993).
48. P. C. Chen et al., "Self-consistent transverse modes in a geometric-phase-plate-assisted optical resonator," *Phys. Rev. A* **105**, 033525 (2022).
49. D. Wei et al., "Generating controllable Laguerre-Gaussian laser modes through intracavity spin-orbital angular momentum conversion of light," *Phys. Rev. Appl.* **11**, 014038 (2019).
50. Y. J. Cai, X. H. Lu, and Q. Lin, "Hollow Gaussian beams and their propagation properties," *Opt. Lett.* **28**, 1084–1086 (2003).
51. A. M. Yao and M. J. Padgett, "Orbital angular momentum: origins, behavior and applications," *Adv. Opt. Photonics* **3**, 161–204 (2011).
52. M. W. Beijersbergen et al., "Helical-wavefront laser beams produced with a spiral phaseplate," *Opt. Commun.* **112**, 321–327 (1994).
53. K. Sueda et al., "Laguerre-Gaussian beam generated with a multilevel spiral phase plate for high intensity laser pulses," *Opt. Express* **12**, 3548–3553 (2004).
54. L. E. Myers et al., "Quasi-phase-matched optical parametric oscillators in bulk periodically poled $LiNbO_3$," *J. Opt. Soc. Am. B* **12**, 2102–2116 (1995).
55. O. Svelto, *Principles of Lasers*, 5th ed., Springer Science +Business Media (2010).
56. J. W. Goodman, *Introduction to Fourier Optics*, 2nd ed., McGraw-Hill Companies (1996).
57. L. Marrucci, C. Manzo, and D. Paparo, "Optical spin-to-orbital angular momentum conversion in inhomogeneous anisotropic media," *Phys. Rev. Lett.* **96**, 163905 (2006).
58. V. Arrizón et al., "Pixelated phase computer holograms for the accurate encoding of scalar complex fields," *J. Opt. Soc. Am. A* **24**, 3500–3507 (2007).

Dunzhao Wei received his PhD in physics from Nanjing University in 2018 and engaged as a researcher in the College of Engineering and Applied Science at Nanjing University. Currently, he has been working as an associate professor in the School of Physics at Sun Yat-sen University since 2019. His research interests include the nonlinear optical effects of micro-nano structured materials and their applications in laser frequency conversion, light field manipulation, and quantum frequency conversion.

Yong Zhang received his PhD from the Department of Physics of Nanjing University in 2007 and engaged in postdoctoral research at Arkansas University in 2008 and 2009. Currently, he is working as a professor at Nanjing University, doctoral supervisor, and head of the Department of Optical Engineering since 2010. His research interests include the new nonlinear and quantum optical effects in micro-nanostructured lithium niobate and other materials, and their applications in laser, imaging, sensing, and precision measurement.

Biographies of the other authors are not available.